Journal of Power Sources 202 (2012) 114–119

Contents lists available at SciVerse ScienceDirect

Journal of Power Sources

journal homepage: www.elsevier.com/locate/jpowsour

# A study of electrically insulated oxide substrates for flat-tube segmented-in-series solid oxide fuel cells

T. Somekawa*, K. Horiuchi, Y. Matsuzaki

*Product Development Dept., Tokyo Gas Co., Ltd., 3-13-1, Minami-senjyu, Arakawa-ku, Tokyo 116-0003, Japan*

ARTICLE INFO

*Article history:*
Received 6 September 2011
Received in revised form
17 November 2011
Accepted 18 November 2011
Available online 8 December 2011

*Keywords:*
Solid oxide fuel cell
Segmented-in-series
Redox
Residual stress, Reforming

ABSTRACT

The reduction and oxidation (redox) durability and reforming activity of MgO–NiO–YSZ composites were examined to evaluate the suitability of MgO–NiO–YSZ composites as support materials for segmented-in-series solid oxide fuel cell (SOFC) cell stacks. The MgO–NiO–YSZ composites were compared with NiO–YSZ composites. The MgO–NiO–YSZ composites showed minimal size and structural changes during redox operations at 800 °C and a nearly equivalent reforming activity to NiO–YSZ composites at temperatures ranging from 600 °C to 800 °C in spite of their lower Ni content. MgO–NiO–YSZ composites are good candidates for the support materials in segmented-in-series (SIS)-type SOFC cell stacks.



## 1. Introduction

Recently, SOFCs have been actively developed as a type of high-efficiency electrical power generation equipment in order to utilise more efficiently the world's remaining limited fossil fuels [1,2]. In Japan, a demonstrative research project on SOFC systems is being carried out to promote the installations of small-scale SOFC systems at such sites as residential houses [3,4]. Under actual load conditions in residential use, natural disasters such as earthquake and lightning strikes, emergency outages caused by blackouts, and local fuel shortages for the anode material can occur. These events expose the anode materials to oxidation conditions. It is well known that re-oxidation of anode materials causes the expansion of the anode material, and re-oxidation sometimes ends up destroying the cell [5–9]. Therefore, it is important to develop SOFCs that are highly resistant to size and structural changes during redox. It has previously been reported that segmented-in-series (SIS)-type SOFCs have a high tolerance to redox [10,11]. Fig. 1 shows a schematic of an SIS-type SOFC [12,13]. In an SIS-type SOFC, multiple single cells are formed on one electrically insulated flat support tube. The electrical current flows longitudinally down one side and flows back along the other side. Fuel gas is supplied to each cell through ducts built inside the porous flat tube. A dense electrolyte covering the flat tube separates the fuel from the air. In order to produce a structure with these characteristics, there are many requirements for the support flat-tube materials used. The materials must be electrically insulating, have enough porosity for effective reactant dispersion, match the coefficient of thermal expansion (CTE) of the other materials, have mechanical strength, and be inexpensive. The support substrate has the largest volume in the cell stack. Therefore, reducing the material cost of the substrate leads to a low-priced SOFC system. In addition to these characteristics, when the substrate has intrinsic reforming abilities, the SOFC system does not need an external reformer, thereby resulting in a simpler design. In this study, we examined the characteristics of MgO–NiO–YSZ (yttria-stabilised zirconia) composites and compared them with NiO–YSZ composites, which are a conventional support in planar-type SOFCs as a reference. In MgO–NiO–YSZ, the low-cost MgO is added to YSZ to match the CTE of the substrate to that of the electrolyte. NiO is added to function as a reformer [14]. However, the addition of NiO causes deterioration in the redox durability. To quantify this deterioration, we examined the characteristics of the tolerance to redox, such as shrinkage changes and residual stress changes, during redox operations and reforming activities for each sample.

## 2. Experimental

### 2.1. Sample preparation

The samples tested were manufactured from commercial ceramics powders using standard ceramic processing techniques. The sample compositions are shown in Table 1. For NiO–YSZ, the samples were prepared using well-mixed powders of NiO (Seido

* Corresponding author. Tel.: +81 3 5604 8275; fax: +81 3 5604 8051.
*E-mail address:* somekawa@tokyo-gas.co.jp (T. Somekawa).

0378-7753/$ – see front matter © 2011 Elsevier B.V. All rights reserved.
doi:10.1016/j.jpowsour.2011.11.056

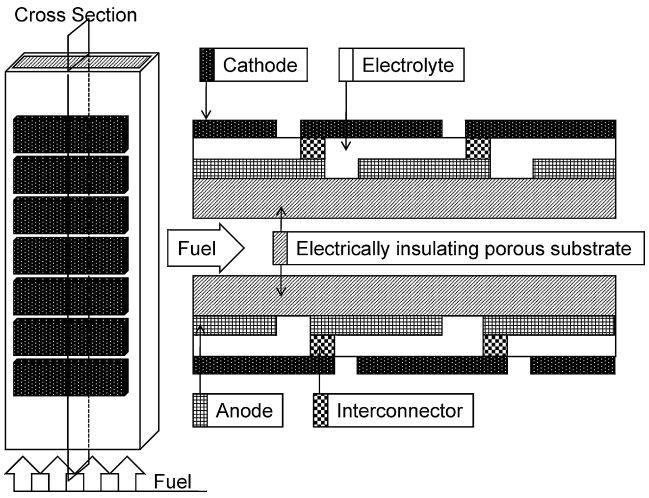


**Fig. 1.** The schematic of a segmented-in-series-type SOFC.

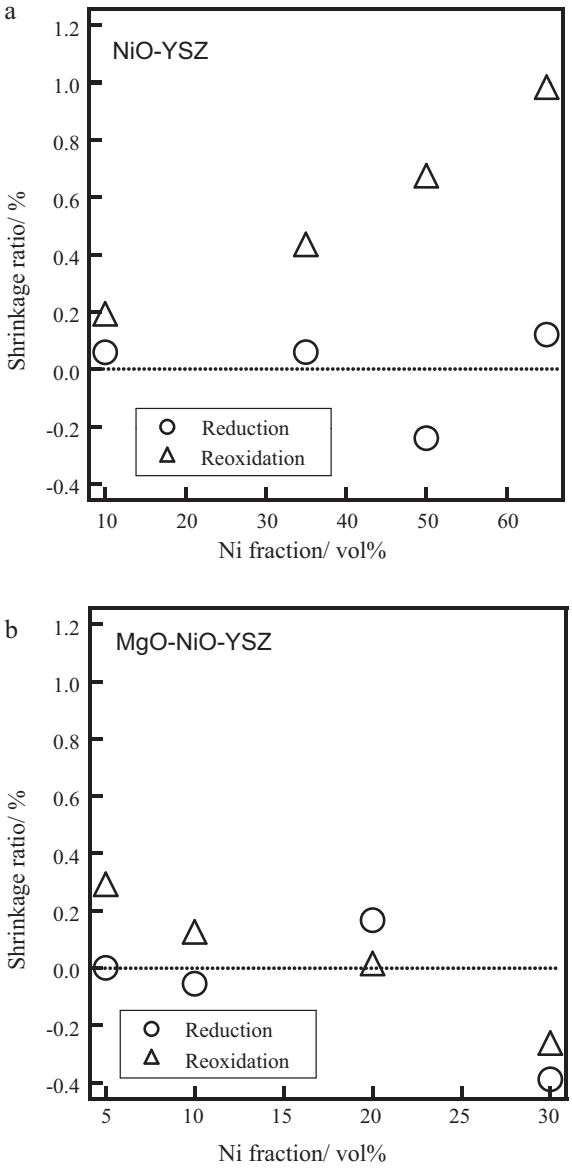


**Fig. 2.** The shrinkage behaviour of samples immediately after calcination at 1500 °C, reduction at 800 °C for 10 h, and re-oxidation at 800 °C for 10 h: (a) the behaviour of NiO–YSZ and (b) the behaviour of MgO–NiO–YSZ.

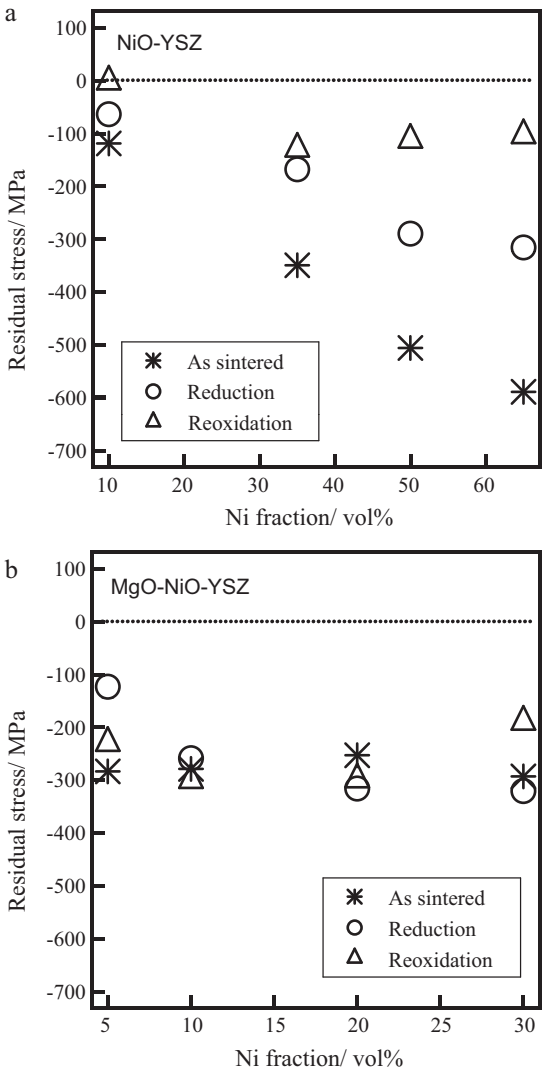


**Fig. 3.** The change in the residual stress on the electrolyte during the redox tests: (a) the behaviour of NiO–YSZ and (b) the behaviour of MgO–NiO–YSZ.

Chemical Industry Corp.) and 8% YSZ (Daiichi Kigenso Kagaku Kogyo Co., Ltd.). For NiO–YSZ–MgO, a (Ni, Mg)O solid solution was initially prepared by calcination of a mixture of MgO powder, which was provided by calcination of $Mg(OH)_2$ powders (Ube Materials Industries, Ltd.) at 1200 °C for 10 h and NiO powder to create a solid solution of (Ni, Mg)O [15,16]. Next, the (Ni, Mg)O was crushed into a powder. After these processes, the MgO–NiO–YSZ physical mixture was prepared. Because higher porosity leads to higher catalytic activity, a pore-forming agent (microcrystalline

**Table 1**
Sample compositions examined in this work.

| Sample name | MgO (vol.%) | NiO (vol.%) | YSZ (vol.%) | Calculated CTE (ppm $K^{-1}$) |
|---|---|---|---|---|
| NY1 | – | 10 | 90 | 10.93 |
| NY2 | – | 35 | 65 | 11.87 |
| NY3 | – | 50 | 50 | 12.36 |
| NY4 | – | 65 | 35 | 12.80 |
| MNY1 | 47.5 | 5 | 47.5 | 12.43 |
| MNY2 | 45 | 10 | 45 | 12.51 |
| MNY3 | 40 | 20 | 40 | 12.66 |
| MNY4 | 35 | 30 | 35 | 12.80 |

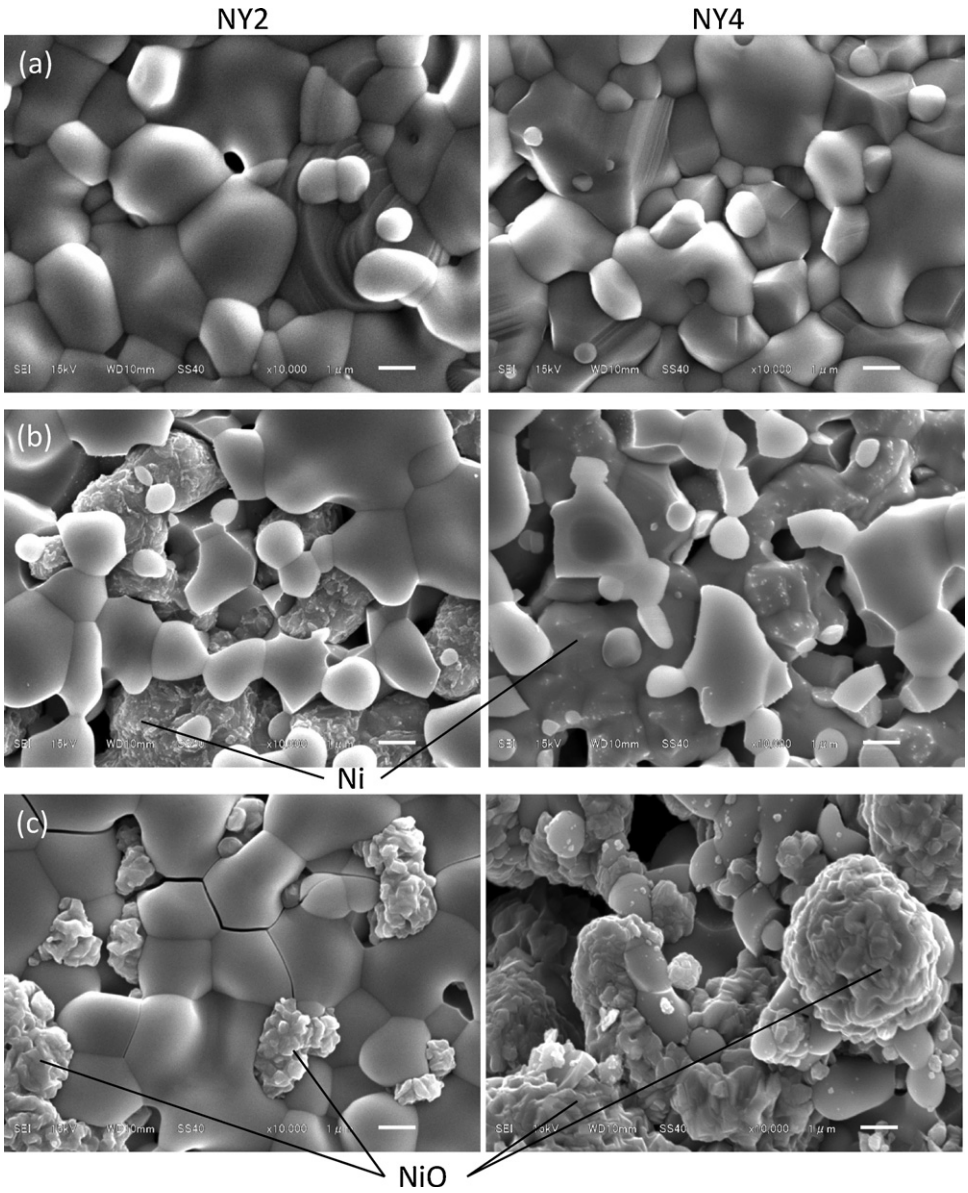


**Fig. 4.** SEM images of the cross sections of NiO–YSZ samples: (a) immediately after calcination at 1500 °C, (b) after the reduction operation at 800 °C for 10 h, and (c) after re-oxidation at 800 °C for 10 h.

cellulose type, Asahi Kasei Corp.) (10%) was added to both mixtures. A solution of 10% polyvinyl butyral (BM-1, Sekisui Chemical Co.) in ethanol was added to prepare pellets without cracks. The powders were well mixed and were pressed uniaxially into circular pellets with a 20 mm diameter at a pressure of 640 kg cm$^{-2}$ for 30 s. The pellets were calcined at 1200 °C for 2 h. Both NiO–YSZ and MgO–NiO–YSZ pellets calcined at 1200 °C were dipped in a YSZ slurry. The samples with an electrolyte layer on the surfaces were subsequently sintered at 1500 °C for 2 h.

### 2.2. Experimental method

#### 2.2.1. Shrinkage behaviour during redox testing

For the shrinkage behaviour tests, the samples were reduced in 4% $H_2$ balanced with $N_2$, and were re-oxidised in air at 800 °C for 10 h. The diameter of each sample was measured by using digital callipers (Mitutoyo Corp.) after sintering, reduction, and re-oxidation.

#### 2.2.2. The measurement of the changes in the residual stress on the electrolyte during the redox test

At each step, we measured the X-ray diffraction pattern of the electrolyte of each sample and estimated the residual stress by the $\sin^2\psi$ method [17–21] with a parallel-beam X-ray diffractometer (Rigaku Corp, RINT-TTR 2) equipped with a Cu target. Regarding the diffracting plane used for the stress measurement, we selected the (5 3 1) plane of 8YSZ [22].

#### 2.2.3. Microstructure observation

After these measurements, the cross-sections of samples were analysed using scanning electron microscopy (SEM, JEOL Ltd., JSM-6510A).

#### 2.2.4. Reforming activity test

Both NY2 and MNY1 samples reduced at 800 °C for 100 h were used for reforming activity tests. In the reforming tests, the steam-to-carbon ratio was constant at 2.0. The tests were carried out at space velocities of 30, 60, and 100/H and temperatures of 600 °C,

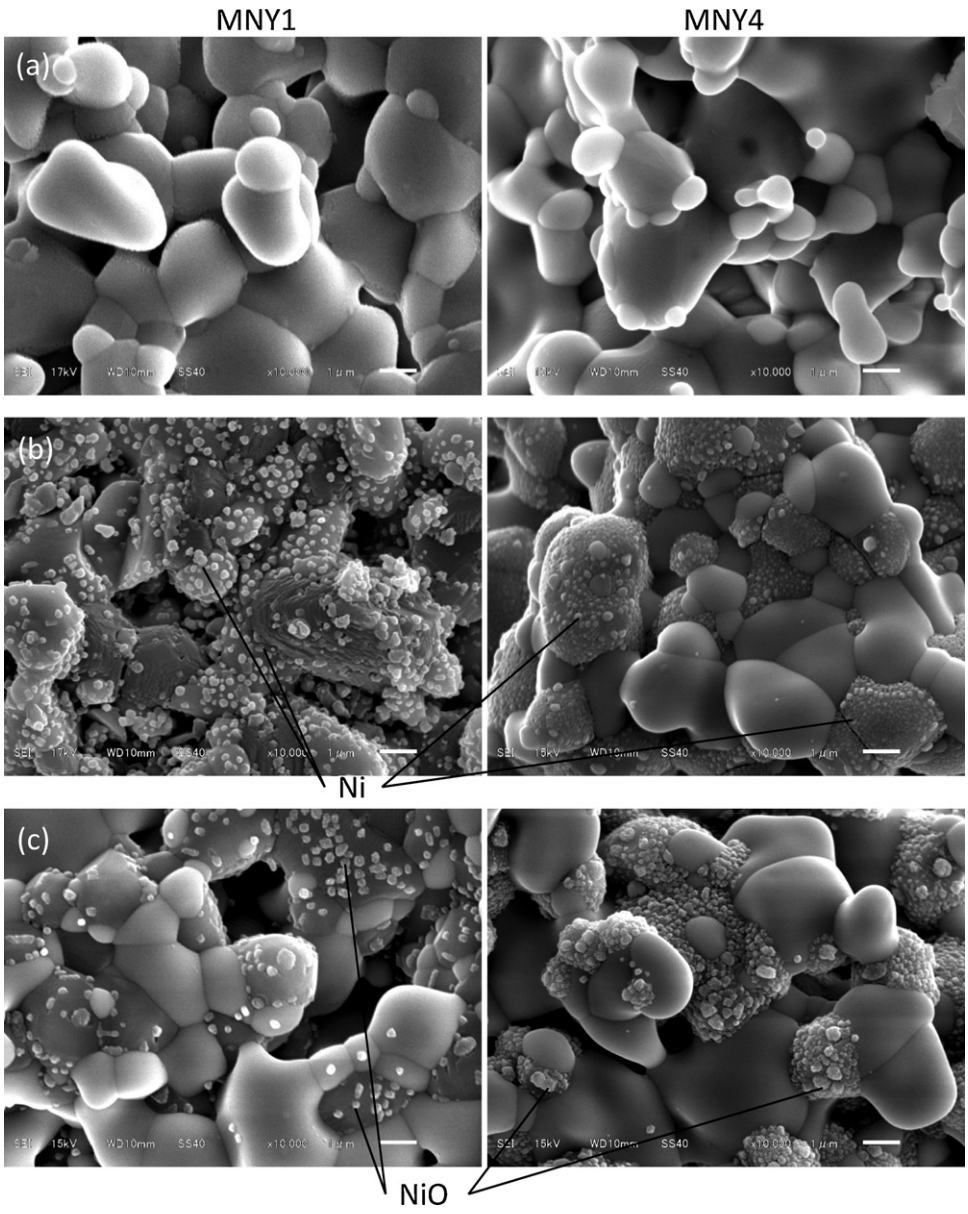


**Fig. 5.** SEM images of the cross-sections of MgO–NiO–YSZ samples: (a) immediately after calcination at 1500 °C, (b) after the reduction operation at 800 °C for 10 h, and (c) after re-oxidation at 800 °C for 10 h.

700 °C, and 800 °C, respectively. After the reforming reactions had occurred, the reforming conversion rates were calculated using the result of gas chromatography (Shimadzu Corp.) analysis. These values were compared with the equilibrium calculation results.

## 3. Results and discussion

### *3.1. Shrinkage behaviour during redox testing*

The shrinkage behaviour of NiO–YSZ and MgO–NiO–YSZ are shown in Fig. 2(a) and (b), respectively. A positive value indicates expansion and a negative value indicates shrinkage. Each plot was calculated based on the size of as-sintered samples. The NiO–YSZ composites showed little size change in terms of reduction, but they expanded during re-oxidation. This expansion occurred because the reduced Ni became NiO. In comparison, the MgO–NiO–YSZ composites showed little size changes in either condition. Concerning the porosities, in NiO–YSZ composites, the porosities increased during the reduction and they decreased during the re-oxidation. In the reduction process, porosities increased in spite of the size shrinkage. This is because the deformation reaction from Ni to NiO, which increased vacancy volume, happened and led to size decrement and porosity increment.

In MgO–NiO–YSZ composites, the porosities of samples stayed at about the same value during both reduction and re-oxidation processes. This is because it was observed that the structures stayed nearly unchanged during the both treatments after the samples were sintered at 1500 °C.

### *3.2. The measurement of the changes in the residual stress on electrolyte during the redox test*

Fig. 3(a) and (b) shows the results of the residual stress measurements of NiO–YSZ and MgO–NiO–YSZ, respectively. A negative value indicates compression stress. In the case of the NiO–YSZ samples, the absolute values of the residual stress increase monotonically with the Ni fraction for the as-sintered condition. As the result of the reduction, the absolute values of the residual

**Table 2**
The details of the results of XRD patterns of powdered NY2 and MNY1 samples.

| Sample name | Detected phase | |
|---|---|---|
| | As-sintered | Reduced |
| NY2 | 8YSZ, NiO | 8YSZ, Ni |
| MNY1 | 8YSZ, (Mg,Ni)O | 8YSZ, Ni, (Mg,Ni)O |

stress decrease. After the re-oxidation, some samples showed a small level of residual stress. This finding is because the samples expanded, and the expansion caused the electrolyte to delaminate from the support. In contrast, in the MgO–NiO–YSZ samples, the residual stresses were approximately 200–300 MPa and were more stable than those of NiO–YSZ samples at each step of the sintering, reduction, and re-oxidation process. This result describes the shrinkage behaviours well. In NiO–YSZ composites, the size changes in samples with high NiO content were bigger than that of low NiO content because the amount of the deformations regarding both reduction and re-oxidation of NiO increased with high NiO content samples. So larger changes in residual stress happened with high NiO content samples than low NiO content samples. In MgO–NiO–YSZ composites, the size changes in each sample during reduction and re-oxidation showed the same tendencies and most of microstructure changes occurred on the surfaces of grains and they had little influence on the size changes. This could be correlated with the almost constant residual stress during both reduction and re-oxidation processes.

### 3.3. Microstructure observation

SEM images of NiO–YSZ and MgO–NiO–YSZ after the redox tests are shown in Figs. 4 and 5, respectively. Image (a) shows the as-synthesised sample, image (b) shows the reduced sample and image (c) shows the re-oxidised sample. The morphology of NiO–YSZ changed drastically from the reduction and re-oxidation processes. These large changes from the re-oxidation reaction were caused when Ni changed into NiO [23–25]. In the MgO–NiO–YSZ samples formed by the reduction of the (Mg, Ni)O solid solution, small particles of Ni metal segregated from the grain of the (Mg, Ni)O solid solution and deposited on the grain surfaces. The re-oxidation process caused the segregated Ni particles to coarsen. MgO–NiO–YSZ composites with different MgO concentration basically showed the same tendencies at each step. From these results, it is estimated that MgO–NiO–YSZ samples maintain a stable size during redox operations.

### 3.4. Reforming activity tests

The methane conversion dependencies of sample NY2 and MNY1 on the temperature and space velocity at a steam-to-carbon ratio of 2.0 are shown in Fig. 6. This finding shows that both NY2 and MNY1 have good reforming activity. In particular, MNY1 exhibits good reforming characteristics in spite of having lower Ni content than that of the NY2 sample. The catalytic reaction progressed rapidly as a function of the space velocities in this measurement.

From these results, it was determined that the MgO–NiO–YSZ samples had size stability in the redox tests and a high reforming activity in spite of the small quantity of Ni they contained. One of the reasons why MgO–NiO–YSZ composites showed good reforming activity in spite of a low Ni content is that they contained nano-scale particles of Ni, which were created by the reduction process. The nano-scale particles can be seen in the SEM image in Fig. 5(b). At this stage, the reason of nano particle Ni formation is not clear. However, Iguchi and Hirao [26] reported the reason of the small size Ni formation from NiO–MgO solid solution by using Ilscher's one-dimensional model [27] for metal formation during the reduction of

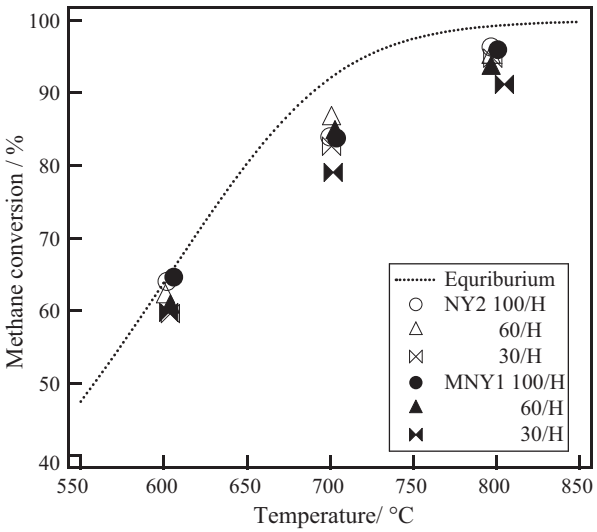


**Fig. 6.** The methane conversion dependence of samples NY2 and MNY1 on the temperature and space velocity at S/C 2.0. The dashed line represents the calculated equilibrium state.

metal-oxide. According to the model, the spacing between nuclei of the metal increases, as the vacancy fraction in the oxide increases. Figs. 7 and 8 show the XRD patterns of NY2 and MNY1, respectively. The (a) line shows the XRD patterns measured immediately after the calcination at 1500 °C, and the (b) line shows those measured after the reduction. Table 2 shows the phases of NY2 and MNY1 detected during the measurement. Table 3 shows the reduction rate, the change in the specific surface area, and the specific surface area of Ni after the reduction at 800 °C for 100 h. The reduction rate was calculated using the data on the mass decrease caused by the reduction of NiO into Ni. In the calculation, all mass decreases were assumed to be caused by the reduction of NiO into Ni. The specific surface area of Ni was calculated from the reduction rate and the change in the measured specific surface area. In the NiO–YSZ samples, almost all of the NiO particles were reduced to Ni. On the other hand, the grate mass of NiO in the (Mg, Ni)O solid solution in MgO–NiO–YSZ was not reduced. However, the calculated value of the specific surface area of Ni in the MNY1 sample increased significantly due to the reduction process. This result also indicates that the reduced MNY1 sample contained small particles of Ni, which indicates a large specific surface area. This finding explains why

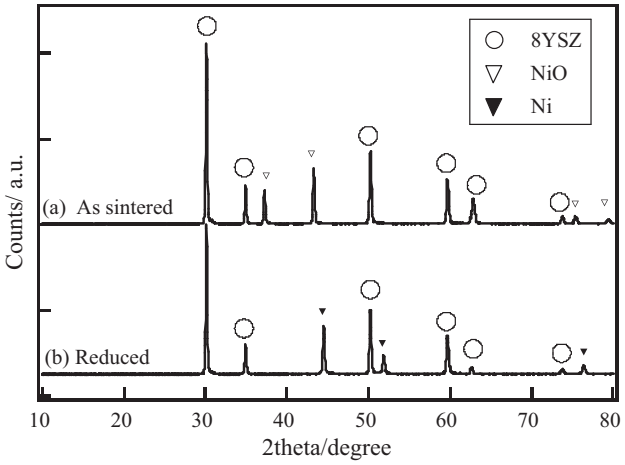


**Fig. 7.** XRD patterns of powdered NY2: (a) immediately after calcination at 1500 °C and (b) after the reduction operation at 800 °C for 100 h.

**Table 3**
The characteristics of samples after reduction operation.

| Sample name | Reduced NiO (%) | Specific surface area change ($m^2\ g^{-1}$) | Specific surface area of Ni particle ($m^2\ g^{-1}$) | Resistivity at 800 °C ($\Omega$ cm) |
|---|---|---|---|---|
| NY2 | 98.5 | 0.092 | 0.278 | $5.0 \times 10^{-2}$ |
| MNY1 | 19.8 | 0.022 | 1.987 | $4.0 \times 10^{5}$ |

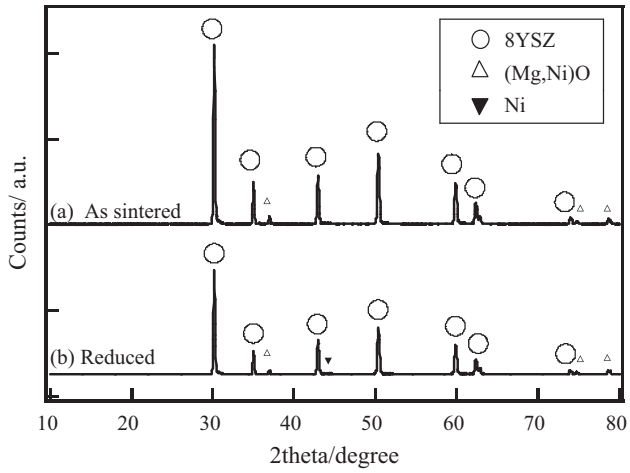


**Fig. 8.** XRD patterns of powdered MNY1: (a) immediately after calcination at 1500 °C and (b) after the reduction operation at 800 °C for 100 h.

MNY1 demonstrated good reforming activity in spite of the low Ni content.

## 4. Conclusion

The durability and reforming activity of MgO–NiO–YSZ and NiO–YSZ as references were investigated. MgO–NiO–YSZ composites showed the following characteristics.

(a) The composites showed less change in size and residual stress in the redox tests at 800 °C.
(b) The composites demonstrated good reforming activity in spite of a low Ni content.
(c) Small particles of Ni metal with a large BET that segregated from the grains of the (Mg, Ni)O solid solution contributed to the high reforming activity.

These results indicate that MgO–NiO–YSZ composites combine a high tolerance for redox processes and a high reforming activity and that they are good candidates to be support materials in SIS-type SOFC cell stacks.

## References

[1] H. Yokokawa, ECS Trans. 35 (1) (2011) 207–216.
[2] K. Horiuchi, K. Nakamura, Y. Matsuzaki, S. Yamashita, T. Horita, H. Kishimoto, K. Yamaji, H. Yokokawa, ECS Trans. 35 (1) (2011) 217–223.
[3] K. Hosoi, M. Ito, M. Fukae, ECS Trans. 35 (1) (2011) 11–18.
[4] H. Yoshida, T. Seyama, T. Sobue, S. Yamashita, ECS Trans. 35 (1) (2011) 97–103.
[5] M. Ettler, N.H. Mezler, H.P. Buchkremer, D. Stöver, Cer. Eng. Sci. Proc. 29 (3) (2008) 33–44.
[6] D. Waldbilling, A. Wood, D.G. Ivey, Solid State Ionics 176 (2005) 847–859.
[7] V. Vedasri, J.L. Young, V.I. Briss, J. Power Sources 195 (2010) 5534–5542.
[8] T. Klemensø, C. Chung, P.H. Larsen, M. Mogensen, J. Electrochem. Soc. 152 (11) (2005) A2186–A2192.
[9] T. Klemensø, B.F. Sørensen, Cer. Eng. Sci. Proc 29 (5) (2009) 81–92.
[10] K. Fujita, T. Somekawa, K. Horiuchi, Y. Matsuzaki, J. Power Sources 193 (2009) 130–13555.
[11] T. Somekawa, K. Fujita, H. Yakabe, Y. Matsuzaki, Proceedings of 35th International Conference on Exposition on Advanced Ceramics and Composites, Daytona Beach, FL, USA, January 23–28, 2011, p. 40.
[12] Y. Matsuzaki, T. Hatae, S. Yamashita, ECS Trans. 25 (2) (2009) 159–166.
[13] T. Ito, Y. Matsuzaki, Proceedings of 34th International Conference on Exposition on Advanced Ceramics and Composites, Daytona Beach, FL, USA, January 24–29, 2010, p. 40.
[14] O. Yamazaki, K. Tomishige, K. Fujimoto, Appl. Catal. A: Gen. 136 (1) (1996) 49–56.
[15] F. Arena, A. Licciardello, A. Parmaliana, Catal. Lett. 6 (1) (1990) 139–149.
[16] F. Arena, A. Parmaliana, N. Mondello, F. Frusteri, N. Giordano, Langmuir 7 (8) (1991) 1555–1557.
[17] I.C. Noyman, J.B. Cohen, Mater. Sci. Eng. 75 (1983) 179.
[18] I.C. Noyman, J.B. Cohen, Adv. X-ray Anal. 27 (1984) 129.
[19] K. Tanaka, Y. Yamamori, N. Mine, K. Suzuki, Proceedings of the 32nd Japan Congress on Materials Research, 1989, p. 199.
[20] Y. Yoshioka, Adv. X-ray Anal. 24 (1981) 167.
[21] M. Barral, J.M. Sprauel, J. Lebrun, G. Maeder, S. Magtert, Adv. X-ray Anal. 27 (1984) 149.
[22] H. Yakabe, Y. Baba, T. Sakurai, Y. Yoshitaka, J. Power Sources 135 (1/2) (2004) 9–16.
[23] T. Klemensø, C.C. Appel, M. Mogensen, Electrochem. Solid-State Lett. 9 (9) (2006) A403–A407.
[24] D. Sarantaridis, R.J. Chater, A. Atkinson, J. Electrochem. Soc. 155 (5) (2008) B467–B472.
[25] T. Hatae, Y. Matsuzaki, S. Yamashita, Y. Yamazaki, J. Electrochem. Soc. 157 (5) (2010) B650–B654.
[26] Y. Iguchi, J. Hirao, J. Japan Inst. Met. 48 (8) (1984) 802–807.
[27] B. Ilschner, Z. Metallkd. 55 (1964) 153.